# Infrared Spectroscopy of $CO_2$ Transformation by Group 3 Metal Monoxide Cations

Dong Yang,[a,b,#] Mingzhi Su,[a,b,#] Huijun Zheng,[a,b] Zhi Zhao,[a] Xiangtao Kong,[a] Gang Li,[a] Hua Xie,[a] Weiqing Zhang,[a] Hongjun Fan,*[,a] and Ling Jiang*[,a]

a. State Key Laboratory of Molecular Reaction Dynamics, Collaborative Innovation Center of Chemistry for Energy and Materials, Dalian Institute of Chemical Physics, Chinese Academy of Sciences, 457 Zhongshan Road, Dalian 116023, China.

b. University of Chinese Academy of Sciences, 19A Yuquan Road, Beijing 100049, China

*E-mail address: ljiang@dicp.ac.cn (L.J.), fanhj@dicp.ac.cn (H.F.).

[#] These authors contributed equally to this work.

**Abstract:** Infrared photodissociation spectroscopy of mass-selected $[MO(CO_2)_n]^+$ (M = Sc, Y, La) complexes indicate that the conversion from the solvated structure into carbonate one can be achieved by the $ScO^+$ cation at $n$ = 5 and by the $YO^+$ cation at $n$ = 4, while only the solvated structures are observed for the $LaO^+$ cation. These findings suggest that both the $ScO^+$ and $YO^+$ cations are able to fix $CO_2$ into carbonate. Quantum chemical calculations are performed on $[MO(CO_2)_n]^+$ to identify the structures of the low-lying isomers and to assign the observed spectral features. Theoretical analyses show that the $[YO(CO_2)_n]^+$ complex has the smallest barrier for the conversion from the solvated structure into carbonate one, while $[LaO(CO_2)_n]^+$ exhibits the largest conversion barrier among the three metal oxide cations. The present system affords a model in clarifying the effect of different metals in catalytic $CO_2$ transformation at the molecular level.

# 1. Introduction

The chemical conversion and fixation of carbon dioxide is one of the most extensively studied catalytic reactions because of their great environmental significance in global warming mitigation and various promising applications in synthetic and material chemistry [1-3]. Metal compounds play an important role in the catalytic transformation of $CO_2$ [4, 5]. Gas-phase optical spectroscopy of mass-selected clusters has provided great insights into the single-site catalysis processes at the molecular level [6-10].

The monodentate coordination M($\eta^1$-$CO_2$), bidentate coordination M($\eta^2$-$CO_2$), or inserted OMCO structures have been observed in the neutral metal-$CO_2$ complexes [6, 11, 12]. In general, the weakly-bound $M^+$-OCO structure is dominated in the interaction of $CO_2$ with a metal cation [7, 13-23]. Interestingly, the metal oxide-carbonyls $[OMCO(CO_2)_{n-1}]^+$ (M = Ti, Ni, Si) present in the $n \geq 5$ clusters [16-18] and a bent $CO_2^-$ fashion appears in $[V(CO_2)_n]^+$ ($n \geq 7$) [20, 24]. In the $[M(CO_2)_n]^-$ cluster anions, the activation of $CO_2$ is very effectively achieved by the excess electron of the metal anion [8, 10, 25-35]. While the bidentate $[M(\eta^2\text{-}CO_2)]^-$ configuration is preferred for the first-row transition metal anions, the metalloformate $[M(\eta^1\text{-}CO_2)]^-$ structure is favored for the $Bi^-$, $Cu^-$, $Ag^-$, and $Au^-$ anions [25, 26, 28, 30]. A oxalate motif has ever been captured in the $[Bi(CO_2)_n]^-$ ($n \geq 5$) clusters [30]. Notable $CO_2$ activation is accessed in a Ni(I) compound [36] and a $[ClMg(\eta^2\text{-}O_2C)]^-$ complex [37].

Recent studies have shown that group 3 metal oxides are promising candidates for catalytic applications [2, 38, 39]. The reaction of $YO^+$ with $CO_2$ was studied using Ion beam mass spectrometry and its bond dissociation energy was measured to be 0.89±0.05 eV by collisional activation experiments with Xe [40]. Collision-induced dissociation experiments indicated that the $[YO(CO_2)]^+$ complex consists of a weakly-bound structure [40]. Infrared photodissociation (IRPD) spectroscopic studies of $[YO(CO_2)_n]^+$ reveal that the first three $CO_2$ molecules are weakly bound to $YO^+$ and a carbonate motif is formed in the $n \geq 4$ clusters, which occurs via a

solvation-induced electron transfer from the ligands to metal [41]. IRPD spectra of the $[NbO_2(CO_2)_n]^+$ and $[TaO_2(CO_2)_n]^+$ cluster cations show the dominant solvated structures, with some characteristic features of a possible carbonate moiety in the $n \geq 4$ clusters [42]. In the $[TiO(CO_2)_n]^-$ cluster anions, the formation of carbonat, oxalato, oxo, $\eta^2$-(O,O), and carbonyl ligands was identified [35]. Matrix-isolation IR spectroscopy of the neutral ScO with $CO_2$ has characterized a carbonate $ScCO_3$ complex [43]. Herein, we report an IR study on the interaction of $CO_2$ with the $ScO^+$ and $LaO^+$ cations using the IRPD spectroscopy and quantum chemical calculations. Combined with the preliminary study of the $[YO(CO_2)_n]^+$ system [41], the systematic experimental results show that $CO_2$ can be converted into carbonate by the $ScO^+$ and $YO^+$ cations instead of $LaO^+$, which is supported by theoretical calculations.

## 2. Experimental method

IR spectra of the $[MO(CO_2)_n]^+$ (M = Sc and La) clusters are measured using an IRPD apparatus, which has been previously described in detail [41, 44]. The $[MO(CO_2)_n]^+$ complexes are prepared by a pulsed laser vaporization source with supersonic expansion of 2% $O_2$ seeded in $CO_2$. The cluster cations of interest are mass-selected and decelerated into the extraction region of a time-of-flight (TOF) mass spectrometer. Here, they interact with a single pass of the IR laser from a Laservision OPO/OPA IR laser. The photodissociation fragments and parent cations are analyzed using the TOF mass spectrometer. Typical spectra are recorded by scanning the infrared laser in step of 2 $cm^{-1}$. The IRPD spectra are acquired by monitoring the fragment ions as a function of the wavelength of tunable infrared laser.

### 3. Theoretical method

Electronic structure calculations are carried out using the Gaussian 09 program [45]. Recent study of the $[YO(CO_2)_n]^+$ complexes has shown that the B3LYP functional augmented with a dispersion correction (B3LYP-D) is able to reproduce the experimental IR spectroscopic observations [41]. Therefore, this functional is ultilized for the present calculations as well. The DZP basis set is used for the carbon,

oxygen, nitrogen, and hydrogen atoms, and the LanL2DZ ECP basis set for the scandium, yttrium, and lanthanum atoms. Tight convergence of the optimization and the self-consistent field procedures is imposed, and an ultrafine grid is used. To obtain relative energies and conversion barriers, the single point calculations are carried out at the B2PLYP(full)/def2-TZVP level based on the B3LYP-D/DZP-LanL2DZ optimized structures. The calculated IR spectra are derived from the B3LYP-D scaled harmonic frequencies (scaling factor: 0.964) [41] and are convoluted using a Gaussian line shape function with a 5 $cm^{-1}$ full width at half-maximum (FWHM).

## 4. Results and Discussion

The time–of–flight mass spectra of the products generated by a pulsed laser vaporization of scandium and lanthanum targets under the supersonic expansion are shown in FIGs. S1 and S2 in the Supporting Information, respectively. The metal monoxide–$CO_2$ cationic complexes in the form of $[MO(CO_2)_n]^+$ (M = Sc and La; $n$ = 1–15) are dominated in the mass spectral signals. Additional signals are assigned to the $[M_2O_2(CO_2)_n]^+$ species with relatively weak intensities as compared to $[MO(CO_2)_n]^+$.

FIGs. 1 and 2 show the experimental IR spectra of $[ScO(CO_2)_n]^+$ ($n$ = 2–11) and $[LaO(CO_2)_n]^+$ ($n$ = 1–10), respectively. The only fragmentation pathways observed involve loss of $CO_2$. The nearly linear laser power dependence of the fragmentation signal is confirmed and the IR spectra are normalized according to the IR power. Band positions of $[MO(CO_2)_n]^+$ (M = Sc and La) are listed in Tables 1 and 2, respectively.

In the experimental IR spectra of $[ScO(CO_2)_n]^+$ (FIG. 1), three main features are observed, labeled a–c. Band a is centered around 2364 $cm^{-1}$, which is characteristic of the antisymmetric stretch of $CO_2$ in the first coordination sphere [7, 8, 10, 13-18, 20-23, 41, 42]. Band b is observed around 2348 $cm^{-1}$, which appears as a small shoulder at $n$ = 7 and the intensity is increased in the larger clusters. This band position is characteristic of the antisymmetric stretching vibration of free $CO_2$ (2349

$cm^{-1}$) [7, 8, 10, 20]. Band c is weakly observed at the $n$ = 5 cluster and red-shifts from 1858 $cm^{-1}$ to 1818 $cm^{-1}$ between $[ScO(CO_2)_5]^+$ and $[ScO(CO_2)_{11}]^+$, which is similar to the $[YO(CO_2)_n]^+$ ($n$ = 4–11) with the characteristics of the C–O stretch [41]. In contrast, only one main feature centered around 2360 $cm^{-1}$ (labeled a) appears in the IR spectra of $[LaO(CO_2)_n]^+$ ($n$ = 1–10) (FIG. 2), while no obvious band is observed in the 1000–2200 $cm^{-1}$ region.

To identify the minimum-energy structures and to understand the experimental spectral features, quantum chemical calculations are carried out using the B3LYP-D functional. Optimized structures of the two kinds of isomers for $[MO(CO_2)_n]^+$ (M = Sc and La) are shown in FIG. 3. The calculated IR spectra of $[ScO(CO_2)_n]^+$ ($n$ = 2–8) are depicted in FIG. 4 and those of $[LaO(CO_2)_n]^+$ ($n$ = 1–8) are shown in FIG. S3, respectively. The calculated band positions of $[ScO(CO_2)_n]^+$ and $[LaO(CO_2)_n]^+$ are given in Tables 1 and 2, respectively.

Two binding motifs of solvated and carbonate structures are obtained, which are similar to those reported recently for the $[YO(CO_2)_n]^+$ system [41]. For $[ScO(CO_2)_n]^+$, the solvated structures, labeled $n$S in FIG. 3, are predicted to be lowest in energy for the $n$ = 1–4 clusters; the most stable isomer of the $n$ = 5 cluster consists of a carbonate binding motif (labeled $n$C), which is retained in all of the lowest-energy isomers of the larger clusters. Similar features of minimum-energy structures are obtained for the $[LaO(CO_2)_n]^+$ clusters (FIG. 3). Slight structural difference is found in $[ScO(CO_2)_5]^+$ where one $CO_2$ ligand is coordinated opposite the carbonate or the oxygen on the axis. In contrast, all the four $CO_2$ ligands are bound to the metal in the equatorial plane in $[LaO(CO_2)_5]^+$.

For the $[ScO(CO_2)_n]^+$ ($n$ = 2–8) clusters, the agreement of the experimental IR spectra with the calculated ones (FIGs. 1 and 4), in particular with the relative band positions and the size-dependent trends, is observed, supporting our initial assignments of these bands. The antisymmetric stretching vibrational frequencies of $CO_2$ in the first solvation shell of the most stable isomers are predicted to be centered around 2360 $cm^{-1}$ (Table 1), which are consistent with the experimental values of

band a. In the $[ScO(CO_2)_7]^+$ cluster, an antisymmetric stretch of $CO_2$ in the second solvation shell is calculated to be 2347 $cm^{-1}$, which also appears in the simulated IR spectra of the $n$ = 8 cluster, reproducing the experimental band b. In the calculated IR spectrum of the most stable structure for $[ScO(CO_2)_5]^+$ (5C), the band at 1833 $cm^{-1}$ is due to the C–O stretch of carbonate core, which is consistent with the experimental value of band c (1858 $cm^{-1}$) (Table 1 and FIGs. 1 and 4). The calculated frequency of band c red-shifts from 1833 $cm^{-1}$ to 1798 $cm^{-1}$ in-between the $n$ = 5 and $n$ = 8 clusters, which is in accord with the size-dependent trend observed in the experimental IR spectra.

For the $[LaO(CO_2)_n]^+$ ($n$ = 1–8) clusters, the calculated IR spectra of solvated structures (FIG. S3) are consistent with the experimental spectra (FIG. 2). In the calculated IR spectra of carbonate structures, the predicted C–O stretches of carbonate core are absent in the experimental spectra. It thus appears that the experimental spectra of $[LaO(CO_2)_n]^+$ ($n$ = 1–10) show the evidence of the formation of solvated structures, with the absence of carbonate structures.

The conversion barrier from the solvated structure into carbonate one of $[MO(CO_2)_5]^+$ calculated at the B2PLYP/def2-TZVP level for Sc, Y, and La is 28.9, 14.4, and 32.2 kJ/mol (FIG. 5), respectively. This indicates that the $[YO(CO_2)_5]^+$ complex has the smallest barrier for the conversion from the solvated structure into carbonate one, while $[ScO(CO_2)_5]^+$ exhibits a slightly larger conversion barrier, supporting the experimental observation of coordination-induced $CO_2$ fixation into carbonate by the $ScO^+$ and $YO^+$ cations. Note that the conversion barrier for the $LaO^+(CO_2)_n$ system is not significantly larger than that for $ScO^+$ and $YO^+$, an alternative reason for the absence of carbonate formation in the $LaO^+(CO_2)_n$ system could be that the conversion rate of solvated $[LaO(CO_2)_n]^+$ complex to carbonate $[La(CO_3)(CO_2)_{n-1}]^+$ species is much slower than that of $[ScO(CO_2)_n]^+$ complex to carbonate $[Sc(CO_3)(CO_2)_{n-1}]^+$ species. Recent gas-phase IRPD spectroscopy of the $[Pt_4CO_2]^-$ cluster identified a molecularly-adsorbed isomer instead of a fully-dissociated structure (the global minimum) [33]. Similarly, higher-energy

isomers on the potential energy surface have also been observed in several cluster systems [46, 47].

As analyzed for the $[YO(CO_2)_n]^+$ system [41], the conversion of M=O and $CO_2$ undergoes a 2+2 cycloaddition transition state, and the negative charges on O is beneficial for its nucleophilic attacking to C center of $CO_2$ ligand. The $CO_2$ conversion from the solvated structure into carbonate one is assisted by donating electrons from the ligands to the metal. The conversion barrier decreases with the increase of cluster size. The Mulliken charges of metal and O atoms of the MO unit in the $[MO(CO_2)_n]^+$ solvated structures are given in Table S1. It can be seen from Table S1 that the difference in the Mulliken charge of metal atom is more prominent than that of O atom. The Sc and Y atoms are more electron rich than the La atom, suggesting a more favorable $CO_2$ carbonation, which is consistent with the present experimental observations.

Previous computational studies on the conversion of $[YO(CO_2)L]^+$ to $[Y(CO_3)L]^+$ (L = $H_2O$, $NH_3$, and NHC (N,N′-bis(methyl)imidazol-2-ylidene)) indicated that the carbonation would become easier via the increase of the donating power of the ligand [41]. Further experimental investigation of $CO_2$ transformation in the ligand-doped $[MO(CO_2)L]^+$ systems is in progress. These studies would shed insights into molecular-level understanding of different degrees of activation of small molecules by tuning metals, ligands, cluster sizes, and supporting materials.

## 5. Conclusions

Gas-phase vibrational spectroscopic and theoretical studies on the reaction of $CO_2$ with the $ScO^+$ and $LaO^+$ cations reveal that the $CO_2$ conversion from the solvated structure into carbonate one is observed for $[ScO(CO_2)_n]^+$ at $n$ = 5, while the $CO_2$ molecule is only weakly bound to the metal in $[LaO(CO_2)_n]^+$. Together the recent study of the reaction of $CO_2$ with $YO^+$ [41], it can be found that the $CO_2$ fixation into carbonate is accessible by both $ScO^+$ and $YO^+$ rather than $LaO^+$. Theoretical analyses show that the $[YO(CO_2)_n]^+$ complex has the smallest barrier for the conversion from

solvated structure into carbonate one, while $[LaO(CO_2)_n]^+$ exhibits the largest conversion barrier among the three metal oxide cations. The present system affords a model in clarifying how the coordination induces $CO_2$ fixation into carbonate by different metal oxides, which should have important implications for the single-atom or single-cluster catalytic transformation of carbon dioxide.

## Supporting Information

Mass spectra of $[ScO(CO_2)_n]^+$ and $[LaO(CO_2)_n]^+$ (FIGs. S1 and S2); Calculated IR spectra of the solvated and carbonate isomers for $[LaO(CO_2)_n]^+$ (FIG. S3); The Mulliken charges of metal and O atoms of the MO unit in the $[MO(CO_2)_n]^+$ solvated structures (Table S1).

## Notes

The authors declare no competing financial interest.

## Acknowledgments

This work was supported by the National Natural Science Foundation of China (Grant numbers 21327901, 21673231, 21673234, and 21688102), the Strategic Priority Research Program of Chinese Academy of Sciences (Grant number XDB17000000), and K. C. Wong Education Foundation.

## References

[1] T. Sakakura, J.-C. Choi and H. Yasuda, Chem. Rev. **107**, 2365-2387 (2007).

[2] W. Taifan, J.-F. Boily and J. Baltrusaitis, Surf. Sci. Rep. **71**, 595-671 (2016).

[3] K. Soltys-Brzostek, M. Terlecki, K. Sokolowski and J. Lewinski, Coord. Chem. Rev. **334**, 199-231 (2017).

[4] M. North, R. Pasquale and C. Young, Green Chem. **12**, 1514-1539 (2010).

[5] X.-B. Lu and D. J. Darensbourg, Chem. Soc. Rev. **41**, 1462-1484 (2012).

[6] J. Mascetti, F. Galan and I. Papai, Coord. Chem. Rev. **190**, 557-576 (1999).

[7] N. R. Walker, R. S. Walters and M. A. Duncan, New J. Chem. **29**, 1495-1503 (2005).

[8] J. M. Weber, Int. Rev. Phys. Chem. **33**, 489-519 (2014).

[9] H. Schwarz, Coord. Chem. Rev. **334**, 112-123 (2017).

[10] L. G. Dodson, M. C. Thompson and J. M. Weber, Annu. Rev. Phys. Chem. **69**, 231-252 (2018).

[11] L. Jiang, X.-B. Zhang, S. Han and Q. Xu, Inorg. Chem. **47**, 4826-4831 (2008).

[12] M. F. Zhou and L. Andrews, J. Am. Chem. Soc. **120**, 13230-13239 (1998).

[13] N. R. Walker, G. A. Grieves, R. S. Walters and M. A. Duncan, Chem. Phys. Lett. **380**, 230-236 (2003).

[14] G. Gregoire, N. R. Brinkmann, D. van Heijnsbergen, H. F. Schaefer and M. A. Duncan, J. Phys. Chem. A **107**, 218-227 (2003).

[15] R. S. Walters, N. R. Brinkmann, H. F. Schaefer and M. A. Duncan, J. Phys. Chem. A **107**, 7396-7405 (2003).

[16] N. R. Walker, R. S. Walters, G. A. Grieves and M. A. Duncan, J. Chem. Phys. **121**, 10498-10507 (2004).

[17] J. B. Jaeger, T. D. Jaeger, N. R. Brinkmann, H. F. Schaefer and M. A. Duncan, Can. J. Chem. **82**, 934-946 (2004).

[18] N. R. Walker, R. S. Walters and M. A. Duncan, J. Chem. Phys. **120**, 10037-10045 (2004).

[19] G. K. Koyanagi and D. K. Bohme, J. Phys. Chem. A **110**, 1232-1241 (2006).

[20] A. M. Ricks, A. D. Brathwaite and M. A. Duncan, J. Phys. Chem. A **117**, 11490-11498 (2013).

[21] X.-P. Xing, G.-J. Wang, C.-X. Wang and M.-F. Zhou, Chin. J. Chem. Phys. **26**, 687-693 (2013).

[22] A. Iskra, A. S. Gentleman, A. Kartouzian, M. J. Kent, A. P. Sharp and S. R. Mackenzie, J. Phys. Chem. A **121**, 133-140 (2017).

[23] Z. Zhao, X. Kong, D. Yang, Q. Yuan, H. Xie, H. Fan, J. Zhao and L. Jiang, J. Phys. Chem. A **121**, 3220-3226 (2017).

[24] D. Yang, X. Kong, H. Zheng, M. Su, Z. Zhao, H. Xie, H. Fan, W. Zhang and L. Jiang, J. Phys. Chem. A **123**, 3703-3708 (2019).
[25] B. J. Knurr and J. M. Weber, J. Am. Chem. Soc. **134**, 18804-18808 (2012).
[26] B. J. Knurr and J. M. Weber, J. Phys. Chem. A **117**, 10764-10771 (2013).
[27] B. J. Knurr and J. M. Weber, J. Phys. Chem. A **118**, 4056-4062 (2014).
[28] B. J. Knurr and J. M. Weber, J. Phys. Chem. A **118**, 10246-10251 (2014).
[29] B. J. Knurr and J. M. Weber, J. Phys. Chem. A **118**, 8753-8757 (2014).
[30] M. C. Thompson, J. Ramsay and J. M. Weber, Angew. Chem. Int. Ed. **55**, 15171-15174 (2016).
[31] M. C. Thompson, J. Ramsay and J. M. Weber, J. Phys. Chem. A **121**, 7534-7542 (2017).
[32] M. C. Thompson and J. M. Weber, J. Phys. Chem. A **122**, 3772-3779 (2018).
[33] A. E. Green, J. Justen, W. Schoellkopf, A. S. Gentleman, A. Fielicke and S. R. Mackenzie, Angew. Chem. Int. Ed. **57**, 14822-14826 (2018).
[34] L. G. Dodson, M. C. Thompson and J. M. Weber, J. Phys. Chem. A **122**, 2983-2991 (2018).
[35] L. G. Dodson, M. C. Thompson and J. M. Weber, J. Phys. Chem. A **122**, 6909-6917 (2018).
[36] F. S. Menges, S. M. Craig, N. Toetsch, A. Bloomfield, S. Ghosh, H.-J. Krueger and M. A. Johnson, Angew. Chem. Int. Ed. **55**, 1282-1285 (2016).
[37] G. B. S. Miller, T. K. Esser, H. Knorke, S. Gewinner, W. Schoellkopf, N. Heine, K. R. Asmis and E. Uggerud, Angew. Chem. Int. Ed. **53**, 14407-14410 (2014).
[38] H. J. Freund and M. W. Roberts, Surf. Sci. Rep. **25**, 225-273 (1996).
[39] M. Firouzbakht, M. Schlangen, M. Kaupp and H. Schwarz, J. Catal. **343**, 68-74 (2016).
[40] M. R. Sievers and P. B. Armentrout, Inorg. Chem. **38**, 397-402 (1999).
[41] Z. Zhao, X. Kong, Q. Yuan, H. Xie, D. Yang, J. Zhao, H. Fan and L. Jiang, Phys. Chem. Chem. Phys. **20**, 19314-19320 (2018).
[42] A. Iskra, A. S. Gentleman, E. M. Cunningham and S. R. Mackenzie, Int. J. Mass

spectrom. **435**, 93-100 (2019).

[43] Q. Zhang, H. Qu, M. Chen and M. Zhou, J. Phys. Chem. A **120**, 425-432 (2016).

[44] H. Xie, J. Wang, Z. B. Qin, L. Shi, Z. C. Tang and X. P. Xing, J. Phys. Chem. A **118**, 9380-9385 (2014).

[45] M. J. Frisch, G. W. Trucks, H. B. Schlegel, G. E. Scuseria, M. A. Robb, J. R. Cheeseman, G. Scalmani, V. Barone, B. Mennucci, G. A. Petersson, H. Nakatsuji, M. Caricato, X. Li, H. P. Hratchian, A. F. Izmaylov, J. Bloino, G. Zheng, J. L. Sonnenberg, M. Hada, M. Ehara, K. Toyota, R. Fukuda, J. Hasegawa, M. Ishida, T. Nakajima, Y. Honda, O. Kitao, H. Nakai, T. Vreven, J. A. Montgomery Jr., J. E. Peralta, F. Ogliaro, M. J. Bearpark, J. Heyd, E. N. Brothers, K. N. Kudin, V. N. Staroverov, R. Kobayashi, J. Normand, K. Raghavachari, A. P. Rendell, J. C. Burant, S. S. Iyengar, J. Tomasi, M. Cossi, N. Rega, N. J. Millam, M. Klene, J. E. Knox, J. B. Cross, V. Bakken, C. Adamo, J. Jaramillo, R. Gomperts, R. E. Stratmann, O. Yazyev, A. J. Austin, R. Cammi, C. Pomelli, J. W. Ochterski, R. L. Martin, K. Morokuma, V. G. Zakrzewski, G. A. Voth, P. Salvador, J. J. Dannenberg, S. Dapprich, A. D. Daniels, O. Farkas, J. B. Foresman, J. V. Ortiz, J. Cioslowski and D. J. Fox, (Gaussian, Inc., Wallingford, CT, USA, 2009).

[46] G. E. Douberly, R. E. Miller and S. S. Xantheas, J. Am. Chem. Soc. **139**, 4152-4156 (2017).

[47] D. J. Goebbert, T. Wende, L. Jiang, G. Meijer, A. Sanov and K. R. Asmis, J. Phys. Chem. Lett. **1**, 2465-2469 (2010).

Table 1. Experimental band positions (in $cm^{-1}$), calculated scaled harmonic vibrational frequencies of the lowest-lying isomers, and band assignments for $[ScO(CO_2)_n]^+$ ($n$ = 2–11)

| $n$ | Band a | | Band b | | Band c | |
|---|---|---|---|---|---|---|
| | Exp. | Calc. | Exp. | Calc. | Exp. | Calc. |
| 2 | 2364 | 2370 | – | – | – | – |
| 3 | 2364 | 2366 | – | – | – | – |
| 4 | 2364 | 2365 | – | – | – | – |
| 5 | 2364 | 2366 | – | – | 1858 | 1833 |
| 6 | 2356<br>2366 | 2352<br>2365 | – | – | 1846 | 1828 |
| 7 | 2356<br>2366 | 2353<br>2360 | 2348 | 2347 | 1837 | 1811 |
| 8 | 2354<br>2360<br>2368 | 2354<br>2359<br>2363 | 2348 | 2350 | 1829 | 1798 |
| 9 | 2358<br>2366 | – | 2348 | – | 1823 | – |
| 10 | 2360<br>2380 | – | 2352 | – | 1820 | – |
| 11 | 2360<br>2380 | – | 2350 | – | 1818 | – |
| Assignment | antisymmetric stretch of $CO_2$ in the first solvation shell | | antisymmetric stretch of $CO_2$ in the second solvation shell | | C–O stretch of $CO_3^{2-}$ | |

Table 2. Experimental band positions (in $cm^{-1}$), calculated scaled harmonic vibrational frequencies of the most-likely isomers, and band assignments for $[LaO(CO_2)_n]^+$ ($n$ = 1–10)

| | Band a | |
|---|---|---|
| $n$ | Exp. | Calc. |
| 1 | 2352 | 2369 |
| 2 | 2360 | 2366 |
| 3 | 2358 | 2362 |
| 4 | 2358 | 2362 |
| 5 | 2362 | 2366 |
| 6 | 2350, 2360, 2375 | 2351,2364,2378 |
| 7 | 2356, 2378 | 2360,2380 |
| 8 | 2356, 2380 | – |
| 9 | 2356, 2380 | – |
| 10 | 2356, 2380 | – |
| Assignment | antisymmetric stretch of $CO_2$ in the first solvation shell | |

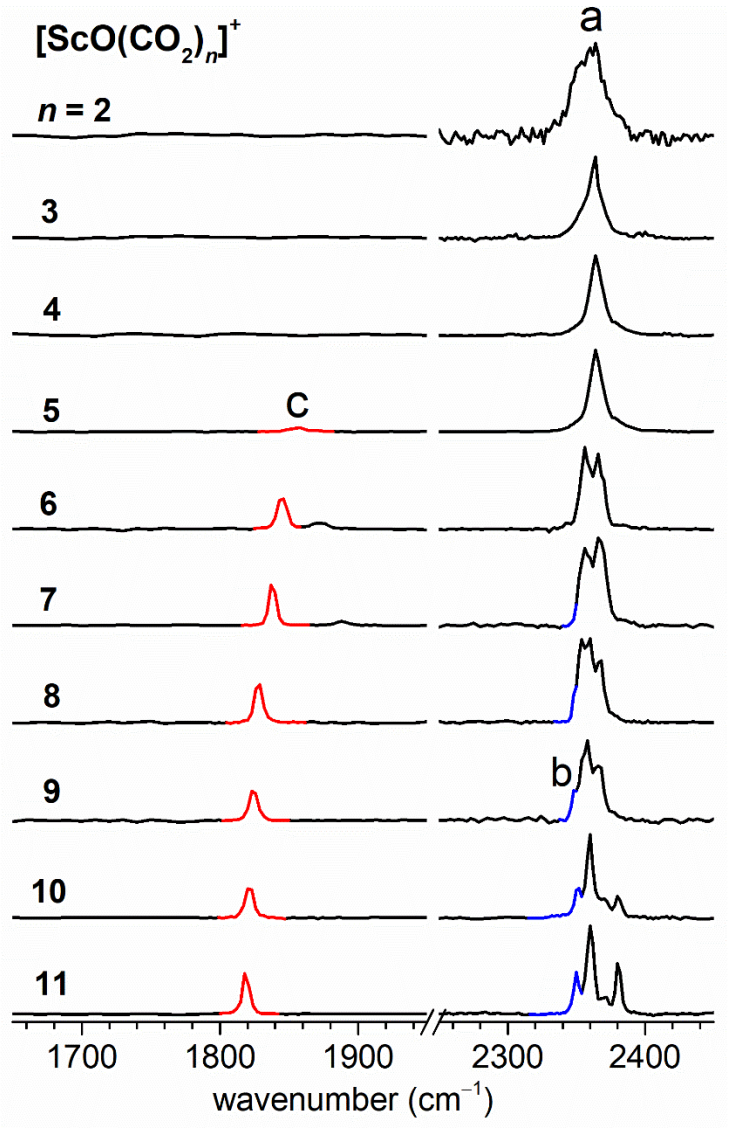


FIG. 1 Experimental IRPD spectra of the $[ScO(CO_2)_n]^+$ ($n$ = 2–11) complexes.

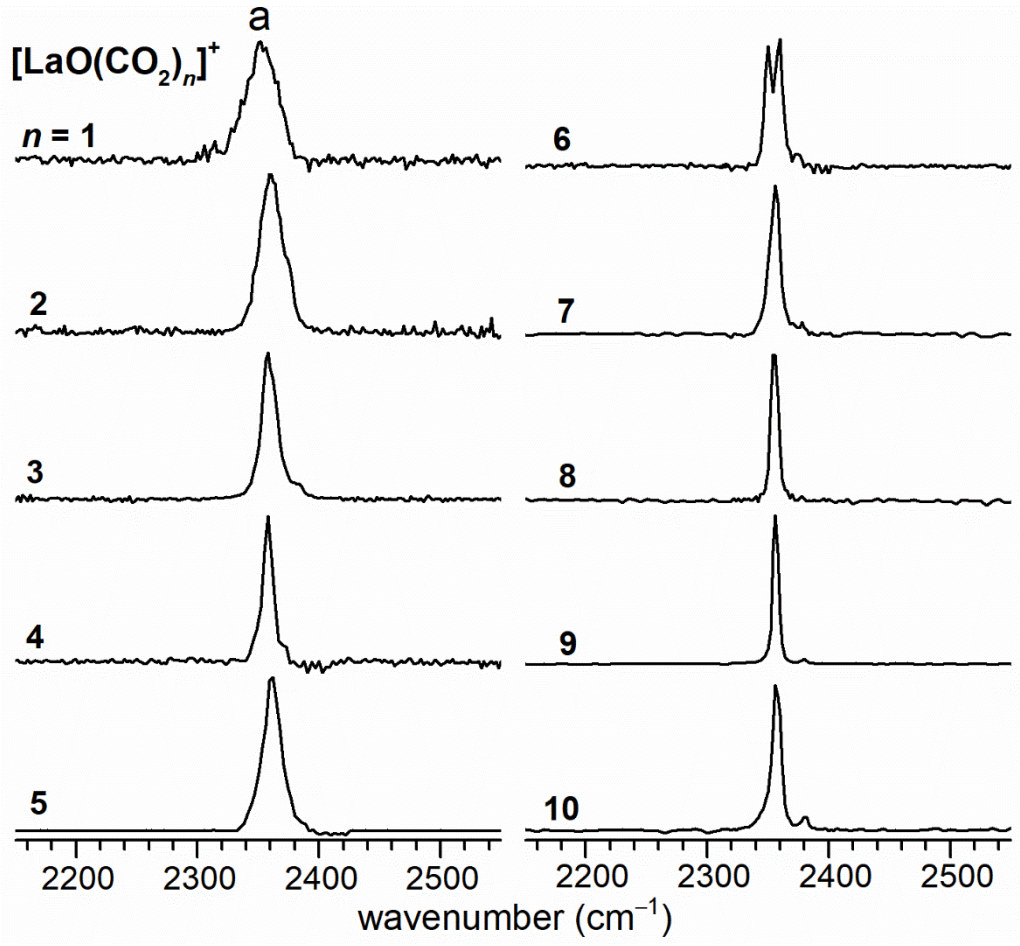


FIG. 2 Experimental IRPD spectra of the $[LaO(CO_2)_n]^+$ ($n$ = 1–10) complexes.

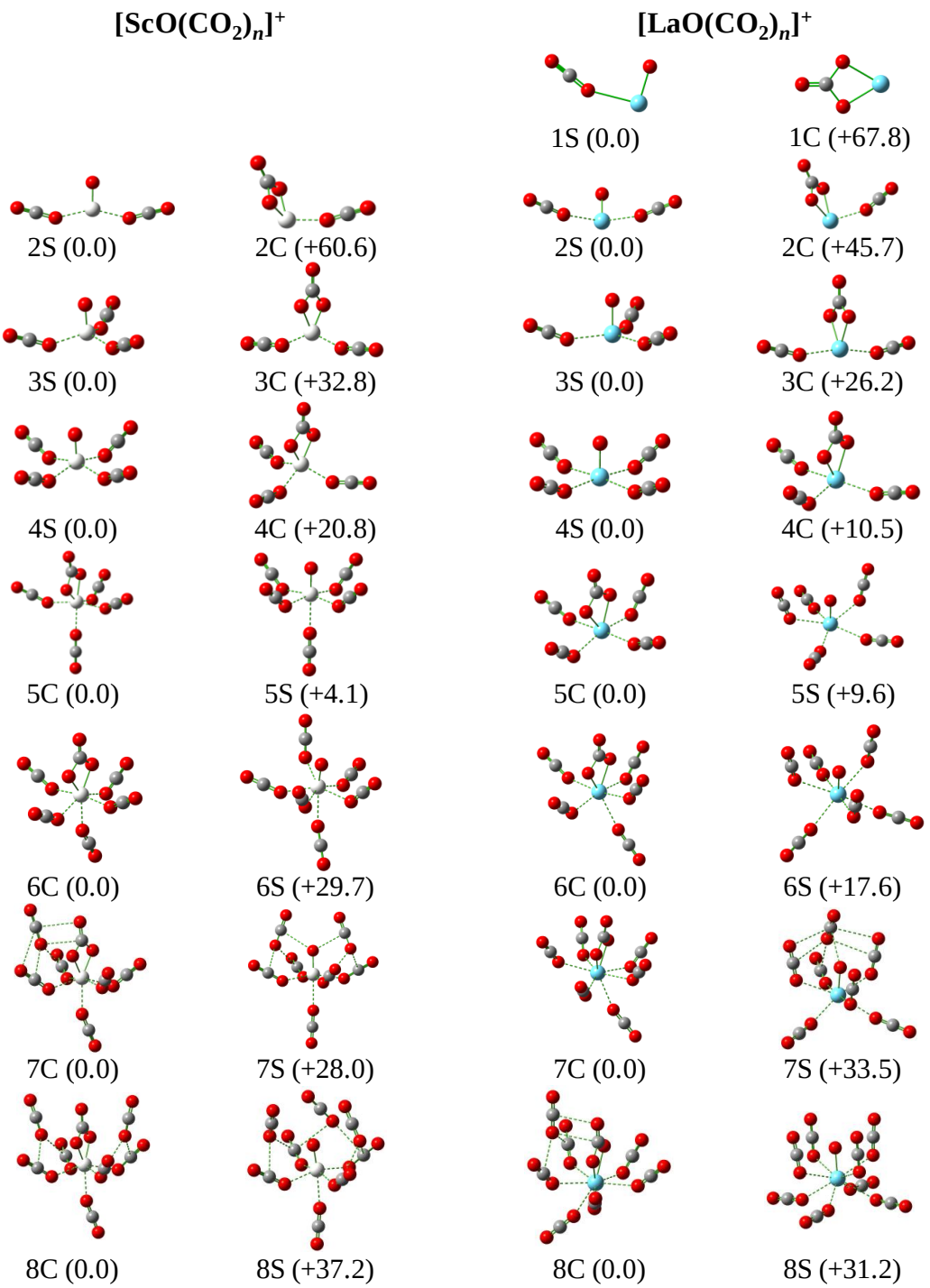


FIG. 3 Representatively optimized structures of the $[ScO(CO_2)_n]^+$ ($n$ = 2–8) and $[LaO(CO_2)_n]^+$ ($n$ = 1–8) complexes (Sc, white; La, cyan; C, gray; O, red). Relative energies are given in kJ/mol.

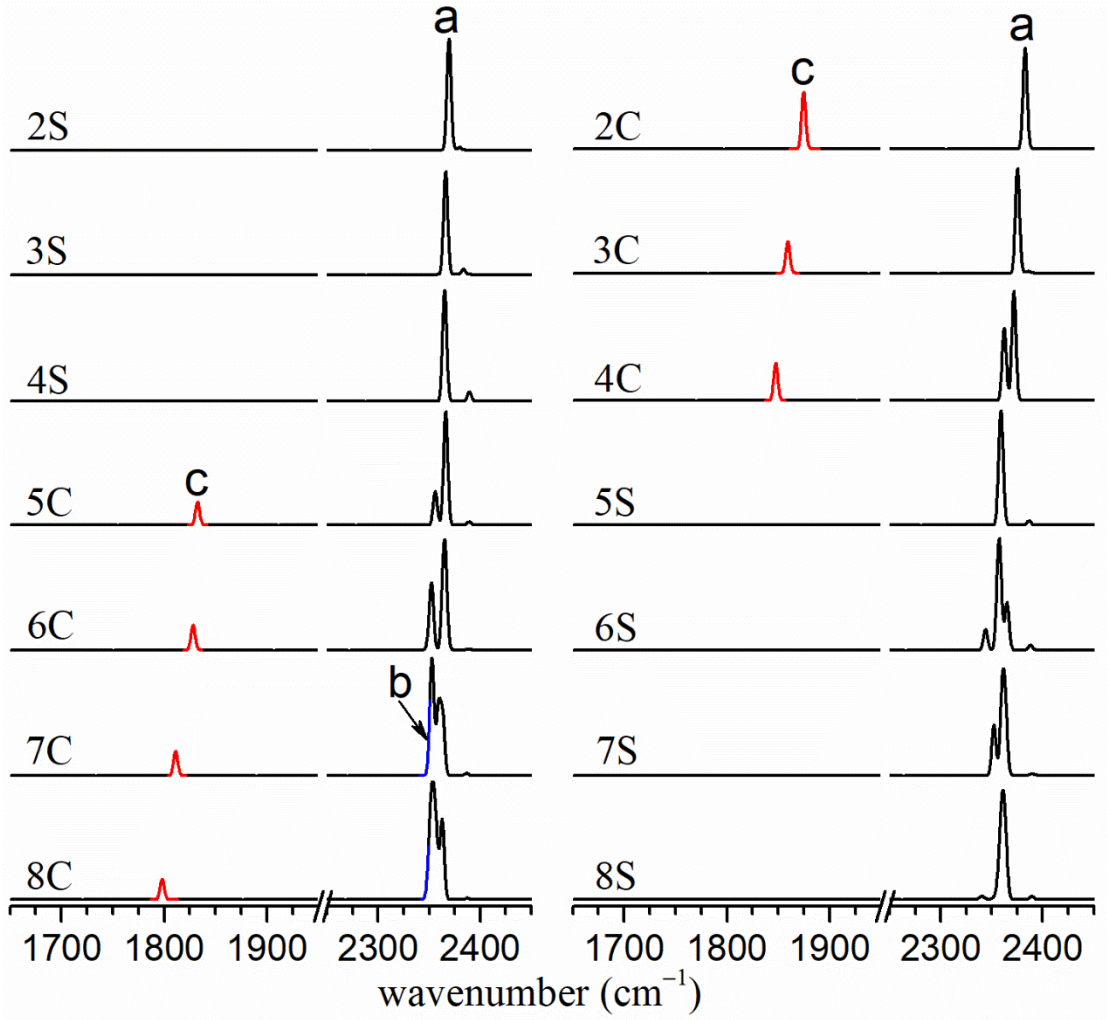


FIG. 4 Calculated IR spectra of the solvated and carbonate isomers for $[ScO(CO_2)_n]^+$ ($n$ = 2–8).

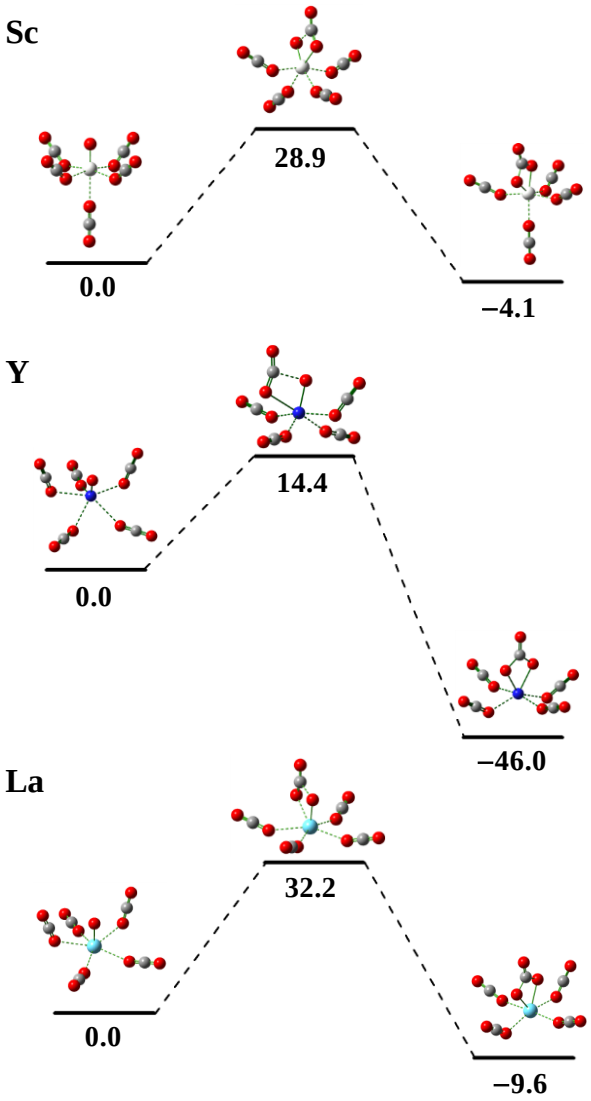


FIG. 5 Potential energy profiles of conversion barrier from solvated structure into carbonate one of $[MO(CO_2)_5]^+$ (M = Sc, Y, La) calculated at the B2PLYP/def2-TZVP level. Energies are given in kJ/mol.